MDPI

Article

Towards an Algorithm for Retrieval of the Parameters of the Marine Atmospheric Boundary Layer at High Wind Speeds Using Collocated Aircraft and Satellite Remote Sensing

Evgeny Poplavsky, Nikita Rusakov, Olga Ermakova *, Daniil Sergeev and Yuliya Troitskaya

Institute of Applied Physics RAS, 603000 Nizhny Novgorod, Russia
* Correspondence: ermakova@ipfran.ru; Tel.: +7-8314164749

Abstract: A method has been developed for the retrieval of the atmospheric boundary layer parameters in tropical cyclones, namely the dynamic speed, the wind speed at a 10 m height, and the roughness parameter. For the analysis, the wind speed profiles were obtained from NOAA GPS-dropsondes and collocated with the data from the Stepped-Frequency Microwave Radiometer (SFMR). The parameters of the atmospheric boundary layer from the GPS-dropsonde data were obtained by taking into account the self-similarity of the velocity defect profile. The emissivity, determined from the radiometric measurement data, was calibrated to the field data from the GPS-dropsondes. Empirical relations between the wind speed, dynamic wind speed, and aerodynamic drag coefficient with the surface emissivity have been proposed. Based on a comparison of the measured dynamic parameters and the surface emissivity, empirical formulas have also been proposed. From an analysis of cross-polarized Sentinel-1 SAR images and collocated SFMR measurements for hurricanes Irma (2017/09/07) and Maria (2017/09/21 and 2017/09/23), we have obtained the dependences of the NRCS on the ocean surface emissivity, surface wind speed, and friction velocity. These results could potentially be used to improve the algorithm for the retrieval of boundary layer parameters in tropical cyclones from remote sensing data.

Keywords: hurricane; microwave remote sensing; atmospheric-ocean boundary layers; wind friction velocity; radiometer; emissivity

1. Introduction

One of the main parameters of the marine boundary layer (MABL) determining the interaction between atmosphere and ocean is the wind stress τ (see extensive reviews in [1,2]), which is often used in atmospheric circulation models for hurricane forecasting:

$$\tau = \rho_a u_*{}^2 \tag{1}$$

where ρ_a is the air density and u_* is the wind friction velocity. It is generally accepted to parametrize the turbulent stress using the drag coefficient and so-called "bulk-formula":

$$\tau = \rho_a C_D U_{10}^2 \tag{2}$$

where C_D is the aerodynamic drag coefficient and U_{10} is the 10 m wind speed. The wind profile for the neutrally stratified atmosphere is:

$$U_{10} = u_*/\kappa \ln(H_{10}/z_0) \tag{3}$$

where κ = 0.4 is the Karman constant, H_{10} is the 10 m height, and z_0 is the roughness parameter, which cannot be measured directly and is usually estimated using U_{10} and u_*. The expressions (1)–(3) show a relation between C_D and the roughness parameter:

$$C_D = \frac{\kappa^2}{\ln^2(H_{10}/z_0)},$$ (4)

A large number of investigations have been conducted to study the dependence of C_D on U_{10} at low and moderate winds [1,3–7]. Initially, it was assumed that C_D is constant, but later, it was found that it increases linearly on wind speed at a height of 10 m for wind speeds up to 20 m/s [8–11]. At the same time experimental investigation demonstrates great uncertainty in the dependence of the drag coefficient C_D on U_{10} at high wind speeds [12–18]. Indeed, it has been demonstrated in [13,14] that the dependence of C_D on U_{10} tends to saturation at wind speeds of 33–35 m/s. It was shown in [12,15,16] that C_D decreases with increasing U_{10} at wind speeds above 30–35 m/s; alternatively, its increase is demonstrated in [17,18], while the level of measurement errors is above 50%. All this leads to significant uncertainties in determining the friction velocity using the bulk formula and has motivated a search for means of the direct measurement of u_*.

Recently, remote sensing microwave instruments have been actively used to retrieve the MABL parameters, as these make it possible to obtain high spatial resolution data on the state of the ocean surface under any weather conditions. For the retrieval of surface wind speed at hurricane wind speeds along with satellite measurements, brightness temperature measurements from the Stepped Frequency Microwave Radiometer (SFMR) installed on research aircraft belonging to the National Oceanic and Atmospheric Administration (NOAA/HRD) [19] during their flight through tropical cyclones is widely used. Based on the obtained measurements of the brightness temperature, the sea surface emissivity is reconstructed, which is determined by the properties of the ocean surface, depending on the surface wind speed. This empirical relationship can be used to retrieve the wind speed from the radiometric measurements.

However, since the emissivity of the sea surface is determined by small-scale roughness, including foam bubbles, spray, etc., it can be expected that the value will be impacted by the wind forcing quantified due to the wind turbulent shear stress (the wind friction velocity). In this regard, the present study is aimed at retrieving the dependence of the emissivity on the shear turbulent stress and the roughness parameter (or drag coefficient.

Recently, there have been studies devoted to creating algorithms for wind speed retrieval from satellite active microwave remote sensing data covering hurricane conditions. It is known that at wind speeds exceeding 25–30 m/s, the sensitivity of the traditionally used co-polarization NRCS (normalized radar cross-section) to wind speed change drops significantly. In this regard, algorithms such as CMOD5 [20] are unsuitable for retrieving wind speed within hurricanes. However, cross-pol NRCS does retain its sensitivity [21–23]. When constructing a geophysical model function relating the cross-pol NRCS to the wind speed, SFMR data are used, along with a few ground data. The possibilities of constructing an algorithm for restoring the friction velocity from satellite cross-pol SAR- images were discussed in [24], where GPS-dropsonde data collocated with the acquisition of cross-pol SAR images were used. The dependencies constructed here, which retrieve the values of the wind friction velocity and the drag coefficient from the airborne SFMR data, provide a significant expansion of the data array compared to the case in which the SAR data are collocated only with GPS-dropsondes.

In this paper, GPS-dropsonde measurements for tropical cyclones and their collocated measurements from SFMR have been used to establish a new geophysical model function (GMF). Section 3 presents a method for retrieval of the wind friction velocity and the roughness parameter based on the analysis of data obtained from GPS-dropsondes; wind velocity profiles are used for the analysis, and an assumption is made about their self-similarity. In Section 4, based on a comparison of data obtained from GPS-dropsondes and SFMR measurements, the empirical dependences of wind speed at a height of 10 m, dynamic wind speed, and the aerodynamic drag coefficient on emissivity are proposed. In Section 5, we obtain the dependencies of the cross-pol NRCS from Sentinel-1 SAR-images on the friction velocity and 10 m wind speed retrieved from the collocated SFMR data

for Category 5 hurricanes. In conclusion, we discuss the dependences obtained and the prospects for their use in remote sensing of the dynamic parameters of the atmosphere.

2. Data

2.1. GPS-Dropsonde Dataset

The data from the NOAA (National Oceanic and Atmospheric Administration) GPS-dropsondes was used to obtain wind speed profiles in tropical cyclones. The datasets are available on the NOAA Hurricane Research mission website (http://www.aoml.noaa.gov/hrd/data_sub/hurr.html (accessed on 14 July 2022)) and contain temperature, pressure, relative humidity, wind speeds, and the corresponding heights measured at 0.5 s resolution. All the data are recorded in ASCII format in AVAPS (Airborne Vertical Atmospheric Profiling System) files for individual GPS-dropsonde. The analysis of wind speed profiles, measured by GPS-dropsondes, was conducted for 25 Category 4 and 5 tropical cyclones (TC) observed in the period from 2001–2017 in the Atlantic basin (see Table 1).

Table 1. Tropical cyclones selected for the analysis and the acquisition time for different instruments.

TC Name	Category	GPS-Dropsondes Launch Time	SFMR Acquisition Time	SAR Acquisition Time
Lili	4	2002/10/02–2002/10/03	2002/10/02–2002/10/03	
Frances	4	2004/08/30–2004/09/02	2004/08/30–2004/09/02	
Dennis	4	2005/07/08–2005/07/10	-	
Ike	4	2008/09/06–2008/09/07	2008/09/06–2008/09/07	
Omar	4	2008/10/16	-	
Paloma	4	2008/11/08	2008/11/08	
Bill	4	2009/08/19–2009/08/20	2009/08/19–2009/08/20	
Fabian	4	2003/09/01–2003/09/05	-	
Gustav	4	2008/08/30–2008/08/31	2008/08/30–2008/08/31	
Earl	4	2010/08/30–2010/09/02	2010/08/30–2010/09/02	
Katia	4	2011/09/06	-	
Gonzalo	4	2014/10/15–2014/10/17	2014/10/15–2014/10/17	
Joaquin	4	2015/10/01–2015/10/02	2015/10/02	
Harvey	4	2017/08/26	-	
Florence	4	2018/09/09–2018/09/12	-	
Jose	4	2017/09/18–2017/09/20	2017/09/19–2017/09/20	
Dean	5	2007/08/16–2007/08/22 (except 2007/08/18)	-	
Irma	5	2017/09/03–2017/09/10	2017/09/04–2017/09/09	2017/09/07
Isabel	5	2003/09/12–2003/09/18	2017/09/09, 2003/09/12	
Ivan	5	2004/09/07–2004/09/15 (except 2004/09/08)	2004/09/09, 2004/09/12–2004/09/15	
Katrina	5	2005/08/26–2005/08/29	2005/08/27–2005/08/28	
Maria	5	2017/09/18–2017/09/27	2017/09/22–2017/09/26	2017/09/21, 2017/09/23
Matthew	5	2016/09/29, 2016/10/01–2016/10/08	2016/09/29, 2016/10/01, 2016/10/04–2016/10/06	
Rita	5	2005/09/19–2005/09/24	2005/09/20–2005/09/23	
Wilma	5	2005/10/18, 2005/10/20–2005/10/24	2005/10/22–2005/10/23	

2.2. SFMR Wind Speed Measurements

Measurements made by the Stepped Frequency Microwave Radiometer (SFMR) are usually synchronized with the launch of the GPS-dropsondes. The SFMR measures brightness temperature at six frequencies (4.55, 5.06, 5.64, 6.34, 6.96, 7.22 GHz) in a 200 MHz bandwidth, from which the ocean surface emissivity is retrieved; it is associated with surface wind speed and precipitation intensity from their contribution to the brightness temperature budget at the specified microwave frequencies. The time period for receiving a dataset from all six channels was 10 s. At a typical aircraft speed of 150 m/s, that corre-

sponds to a spatial resolution of 1.5 km along the flight path. In addition, the cross-scale of the studied area of the ocean surface depends on the flight altitude, the physical dimensions of the antenna, and the frequency of the microwaves. At a typical flight altitude of 1500 m, the transverse scale of the study area has a diameter of 600 to 800 m, depending on the channel. The acquisition time of SFMR data for selected tropical cyclones is presented in Table 1.

2.3. Sentinel-1 Data

In this study, we use the data acquired by the C-SAR radar with the frequency 5.405 GHz of the Sentinel-1 satellite (European Space Agency). The images are usually made for different modes: Wave mode, Stripmap mode, Extrawide Swath mode, and Interferometric Wide Swath mode. The last one was used in the present study at VH cross-polarization. SAR images were collected from the ESA Copernicus Open Acess Hub (https://scihub.copernicus.eu/ (accessed on 14 July 2022)) for the hurricanes Maria (2017/09/18–2017/09/27, Category 5 (SSHS)) and Irma (2017/09/03–2017/09/10, Category 5 (SSHS)) (see Table 1).

3. Retrieval of Atmospheric Boundary Layer Dynamic Parameters from GPS-Dropsonde Data

The generally accepted approach used in technical hydrodynamics to describe turbulent boundary layers in pipes and on flat plates is based on the retrieval of the dynamic wind speed from the airflow velocity profiles averaged over turbulent fluctuations (see [25]). It is assumed that the velocity profiles in the boundary layer are self-similar and can be conditionally subdivided into a logarithmic part (a layer of constant flows) and a "wake" part located above, where the flow adapts to the undisturbed flow [25]. Using the self-similarity property, the parameters of the wind flow (dynamic wind speed, roughness parameter) can be determined from the data obtained in the region of the profile wake part. Based on the proposed approach, it is possible to avoid the effect of velocity profile deformation due to the wave momentum flux (see, for example, [26]), as well as to reduce the high level of errors that are observed in the region of constant fluxes close to the surface where measurements are often missing or inaccurate. In the present paper, the proposed approach is applied to wind speed profiles using NOAA (National Oceanic and Atmospheric Administration) GPS dropsondes for selected tropical cyclones (see Table 1). With these, the problem is especially noticeable for measurements in the vicinity of tropical cyclones, where data loss near the surface is much more significant compared to measurements far from the surface (see [27]).

The self-similar laws mentioned above may be applied only to the statistically averaged turbulent boundary layer velocity profiles, while the individual airflow velocity profiles measured by the GPS-dropsondes demonstrate stochastic behavior on the vertical coordinate and should be grouped into statistical ensembles for further averaging. In the present study, for each hurricane, a selected dataset from GPS-dropsondes (see Table 1) was analyzed, and data obtained for several days and containing high wind speeds were considered. The statistical ensembles were formed from sets of wind velocity profiles selected during the day at approximately the same distance from the hurricane center and demonstrated a similar dependence of wind speed on height. To obtain the statistical ensembles, the selected groups of vertical profiles of the boundary layer velocities measured by the GPS-dropsondes were displayed in three-dimensional coordinates—wind speed, vertical coordinates, and distance from the center of a tropical cyclone. For a visual assessment of the configuration of the statistical ensembles see Figure 1. Such a graphical representation clearly illustrates that profiles with similar qualitative and quantitative characteristics can be conditionally combined into three arrays located at a certain distance from the center of the hurricane: the first array is the profiles grouped inside the eye of the hurricane, with velocities at the upper boundary of the boundary layer less than 20 m/s (red profiles in Figure 1) (they are excluded from the statistical analysis due to low wind speeds); the

second array—GPS-dropsondes with wind speeds at the upper boundary of the boundary layer above 20 m/s (included in the statistical analysis) (green profiles in Figure 1); the third array—GPS-dropsondes that fell in the area of the outer vortex of the hurricanes, at large distances from the center (blue profiles in Figure 1) (also not taken into account when compiling the statistical ensemble due to low wind speeds at the upper boundary of the boundary layer—less than 20 m/s).
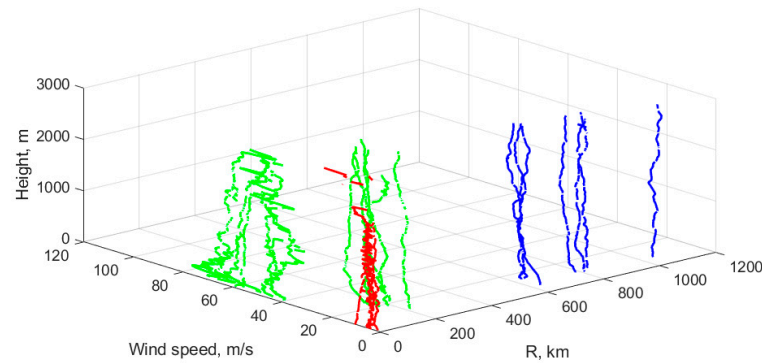

Figure 1. 3-D illustrations, the axes respectively show the distance from the center of the hurricane (obtained by comparing the measurement data of the coordinates of the NOAA GPS-dropsondes and the coordinates of the hurricane's track at the time the GPS-dropsonde fell), with the wind speed and altitude measured by the GPS sensor of the falling GPS-dropsonde. Dataset for hurricane Dean, 2007/08/19. Red profiles correspond to the eye of the tropical cyclone (excluded from the analysis); blue profiles indicate the data obtained far from the tropical cyclone center (wind speeds less than 20 m/s, excluded from the analysis); green profiles represent the data used for the statistical analysis.

As a result, wind speed profiles averaged over the profile groups could be obtained (see Figure 2a).
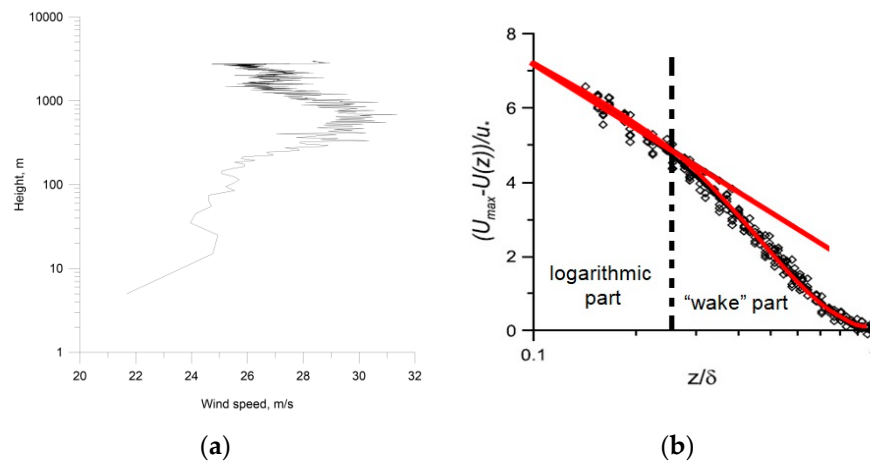

(a) (b)

Figure 2. An example of a wind speed profile averaged over the profile groups for hurricane Katrina 2005/08/27 (**a**); airflow velocity profiles measured by the authors in the aerodynamic flume at different wind speeds over the waves in self-similar variables (reproduced from [28], with permission from John Wiley & Sons, 2012) (**b**). The straight solid line is the logarithmic approximation.

Since the phenomenon of capping inversion is observed above the convective layer in the planetary boundary layer, it can act as a cover, and the atmospheric boundary layer in a tropical cyclone can be considered to be a flow in a channel. Such flows can typically be subdivided into two characteristic regions (see Figure 2b): a layer of constant fluxes, for which the velocity profile is characterized by a logarithmic law with a thickness of $\sim 0.3\delta$ (δ is the thickness of the turbulent boundary layer, [29]) and the wake part, in which the

maximum wind speed is observed (described by a parabolic dependence, see [25]). For a tropical cyclone, the thickness of the turbulent boundary layer is usually about 1 km (see, for example, Figure 2a); consequently, the thickness of the layer of constant fluxes can be estimated as ~300 m. The atmospheric boundary layer in a tropical cyclone as part of the layer of constant fluxes contains a region where momentum is exchanged between the airflow and surface waves, with a scale of $\lambda/10$, where λ is the wavelength [30], so in this region, the sum of turbulent and wave fluxes remains constant [26]. In the case of intense tropical cyclones of categories 4 and 5, when the wavelengths are in the hundreds of meters, the height of the layer containing the wave flux turns out to be of the order of several tens of meters, which means that the logarithmic approximation of the velocity profile is valid only for a narrow range of heights and the method of dynamic velocity retrieval from the logarithmic part of the profile leads to significant errors. In this regard, an approach was developed based on determining the parameters of the boundary layer from the data obtained in the wake part of self-similar velocity profiles. The authors used a similar approach in laboratory experiments on a wind wave flume when measuring the dynamic wind speed [28], which was based on the self-similarity property of the velocity defect profile [25]:

$$\frac{U_{\max} - U(z)}{u_*} = F\left(\frac{z}{\delta}\right), \tag{5}$$

where $U_{\max}$ is the maximum velocity in the turbulent boundary layer and u_* is the friction velocity, δ—the boundary layer thickness. In [25], the following self-similar velocity profile approximation was used for the case of a non-gradient turbulent boundary layer on a flat plate or in a wind channel:

$$U_{\max} - U(z) = \begin{cases} u_*\left(-\frac{1}{\kappa}\ln(z/\delta) + \gamma\right); \ z/\delta < 0.3 \\ \beta u_*(1 - z/\delta)^2; \ z/\delta > 0.3 \end{cases}, \tag{6}$$

where $\kappa = 0.4$ is the von Karman constant and γ, β are the constants; their values will be defined using an algorithm described below. In [13] this method was used for estimation of the atmospheric boundary layer parameters in a hurricane. The parameters $U_{\max}$, u_*, δ included in formula (6) can be easily obtained using the second-degree polynomial approximation of the measured velocity profile in the "wake" part, i.e., at $z/\delta > 0.3$:

$$U(z) = p_3 + p_2 z + p_1 z^2, \tag{7}$$

Comparison with (3) implies relations that make it possible to calculate the parameters of the turbulent boundary layer ($U_{\max}$, u_*, δ):

$$\beta u_* = -\frac{p_2^2}{4p_1}; \delta = -\frac{p_2}{2p_1}; U_{\max} = p_3 + \beta u_*, \tag{8}$$

Figure 2 shows the velocity profiles in the boundary layer which are expressed in the self-similar variables $\frac{U_{max} - U(z)}{\beta u_*}$ and $\frac{z}{\delta}$. These profiles were obtained by averaging the ensemble of velocity profiles realizations measured under approximately the same conditions, similar to the example shown in Figure 1. It is seen from Figure 3 that the velocity profiles expressed in self-similar variables collapse to one curve expressed by Equation (6).

Approximation of the experimental data by formula (6) gives $-1/(\kappa\beta) = 0.3474 \pm 0.014$ while the coefficient $\gamma/\beta = 0.07318$ with 95% confidence lies in the interval from 0.04648 to 0.09988. The friction velocity u_* was calculated from the obtained βu_* (see formula (8)) and β, and then, using the obtained values of $U_{\max}$, u_*, δ the roughness parameter and surface wind speed were determined:

$$z_0 = \delta \exp(-\kappa U_{\max}/u_* + \gamma\kappa)$$
$$U_{10} = 2.5 u_* \ln(H_{10}/z_0) \tag{9}$$

where $H_{10} = 10$ m. And then the aerodynamic drag coefficient can be obtained from (7, 8):

$$C_D = \left(\frac{u_*}{U_{10}}\right)^2 = \frac{\kappa^2}{\left(\kappa U_{\max}/u_* - \gamma\kappa + \ln(H_{10}/\delta)\right)^2},$$ (10)

The surface wind speed obtained in this way is different from the surface wind speed U_{sfc} determined through the average wind speed in the 150-m atmospheric layer (see [19]). Figure 4 shows the relationship between U_{10} and U_{sfc}: $U_{sfc} = 0.83U_{10} + 6.79$. The overall bias, RMSE, and Cor are -0.3506, 4.8148, and 0.91, respectively. It can be seen that U_{10} and U_{sfc} are highly correlated. However, for speeds below 40 m/s, the values are somewhat underestimated, and for speeds above 40 m/s, they are overestimated.
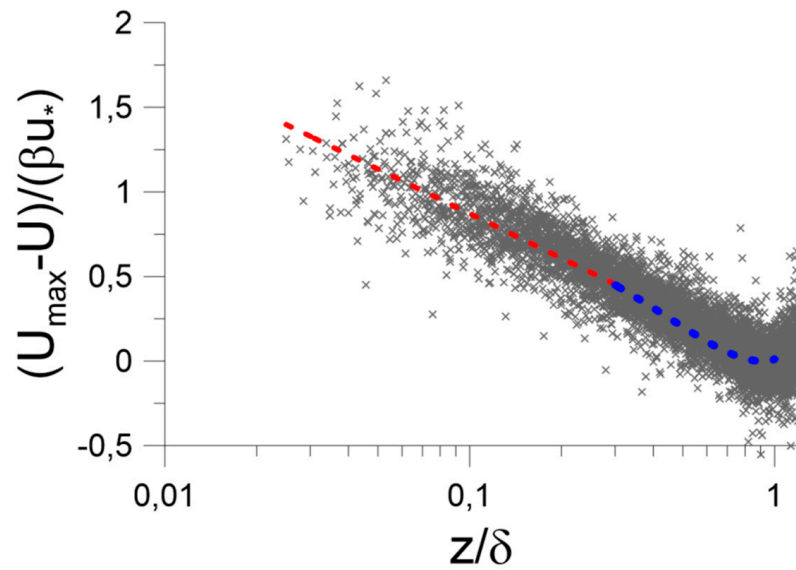

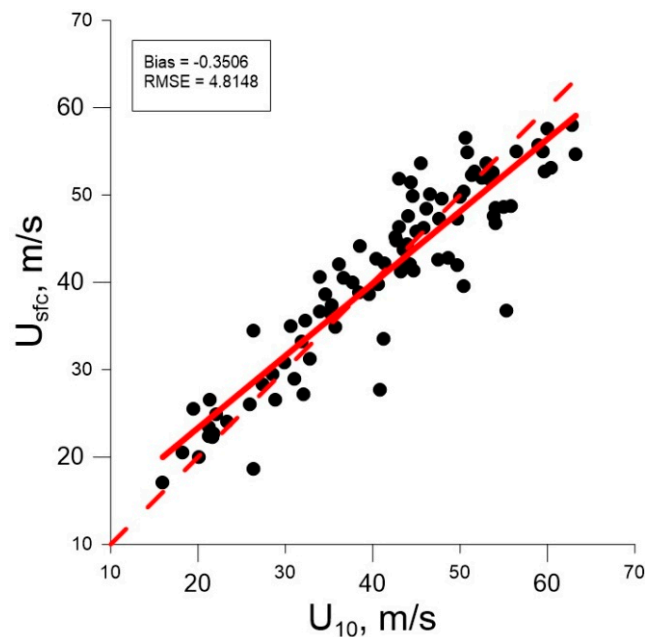**Figure 3.** Velocity profiles in self-similar variables (6).

Figure 4. Comparison of the near-surface wind speed: U_{sfc}, determined in [19] and U_{10} calculated by formula (6), the solid line corresponds to the approximation $U_{sfc} = 0.83U_{10} + 6.79$. Bias $= -0.3506$, RMSE $= 4.8148$, Cor $= 0.91$.

Thus, the estimates of the surface wind speed obtained by the two different approaches appear to be comparatively close. Calculations for individual statistical ensembles constructed from velocity profiles measured under approximately the same conditions were made in order to obtain the values of u_*, C_D, and U_{10}, using Equations (9) and (10). The dependencies of u_* and C_D on U_{10} are shown in Figure 5. The green values were obtained using the procedure of binning, which means that the data was averaged inside the bins for U_{10} with a size of 5 m/s.
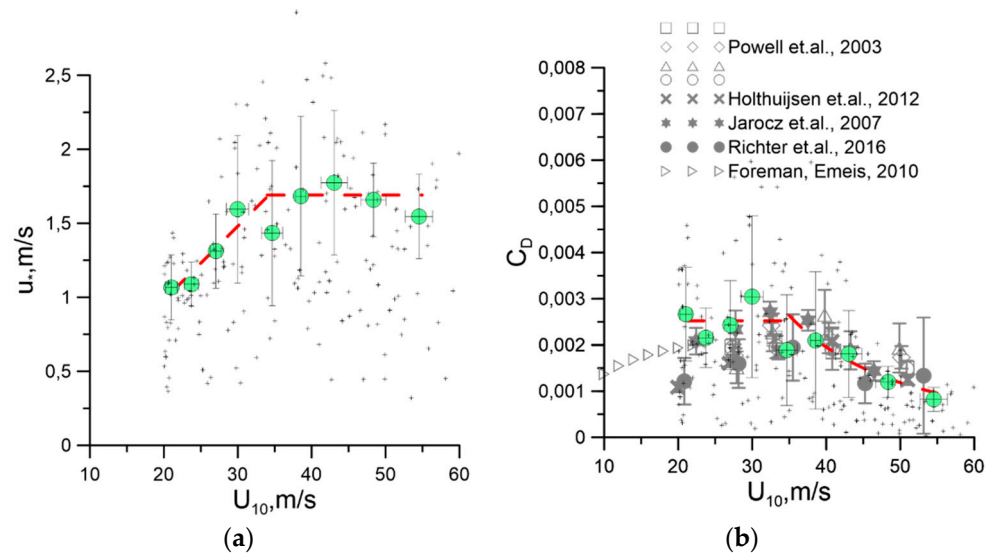

(a)   (b)

Figure 5. Dependence of the wind friction velocity u_* on U_{10} (**a**) and the aerodynamic drag coefficient of the ocean surface on U_{10} (**b**). Black symbols are the results of calculations for individual statistical ensembles, green symbols are averaged values, red lines are power-law approximations. The grey symbols are field measurements from [12,15,16,18,31].

It can be seen from Figure 5 that the dependency of u_* on U_{10} is linear, and the aerodynamic drag coefficient does not change within the experimental error $C_D \approx 0.0025$ for $U_{10} < 35$ m/s. The obtained dependency is in accordance with the result obtained in [31], where it was shown that within the rough flow regime, the neutral friction velocity is linearly dependent on the 10 m wind speed for wind speeds less than 25 m/s. When U_{10} exceeds the threshold of 35 m/s, the dynamic wind speed becomes a constant $u_* \approx 1.70$ m/s within the confidence interval. However, this result needs to be fully verified with a greater amount of data for analysis, so a weak dependence $u_*(U_{10})$ cannot be excluded. For $U_{10} > 35$ m/s, the drag coefficient decreases proportionally to $(U_{10})^{-2}$, and this dependence of $C_D (U_{10})$ is in a good agreement with the data reported in [12,15,16,18,31] (see Figure 4b). Presumably, the anomalous behavior of the dynamic wind speed and associated wind stress at high wind speeds are concerned with the presence of spray in the marine atmospheric boundary layer [30,32], foam at the water surface [33,34], the peculiarities of surface wave form drag (e.g., [35]), etc. However, this problem needs more detailed study in future.

4. Comparison of the Atmospheric Boundary Layer Dynamic Parameters with Values of the Emissivity of the Sea Surface According to SFMR Data

The values of U_{10}, u_*, and C_D obtained from the GPS-dropsondes data were compared with measurements made by the Stepped Frequency Microwave Radiometer (SFMR), which were synchronized with the launch of the GPS-dropsondes.

The principle of the wind speed retrieval method of a tropical cyclone is to use a geophysical model function (GMF) representing the dependency of the ocean surface emissivity E_w on the surface wind speed (see [19]):

$$E_w = \begin{cases} a_1 U_{sfc}, U_{sfc} \leq 7 \text{ m/s}, \\ a_2 + a_3 U_{sfc} + a_4 U_{sfc}^2, 7 \text{ m/s} < U_{sfc} \leq 31.9 \text{ m/s}, \\ a_5 + a_6 U_{sfc}, U_{sfc} > 31.9 \text{ m/s} \end{cases} \tag{11}$$

where the coefficients have the following values:

$$(a_1, a_2, a_3, a_4, a_5, a_6) = (0.0401, 0.2866, -0.0418, 0.0058, -5.6658, 0.3314) \times 10^{-2}, \tag{12}$$

The time series of the U_{sfc} value retrieved using this algorithm can be found at the website (https://www.aoml.noaa.gov/hurricane-research-division (accessed on 14 July 2022)). In the current study, the Formulas (11) and (12) were used to determine the emissivity E_w. It was calculated at the points corresponding to the coordinates of the GPS-dropsondes and then averaged over the GPS-dropsonde groups defined earlier. The obtained E_w values were compared to the U_{10}, u_*, and C_D calculated on the basis of the method proposed in Section 2. To obtain the dependences of the average values of u_*, C_D, and U_{10}, on the mean E_w, the data were grouped (binned) by the E_w value and averaged. The results of such processing are shown in Figure 6. It can be seen (Figure 6a) that, within the error limits, Formula (11) (dashed curve on Figure 6a) describes the experimental data for $U_{10}(E_w)$. In this article, we propose another empirical function $U_{10}(E_w)$ representing two power approximations:

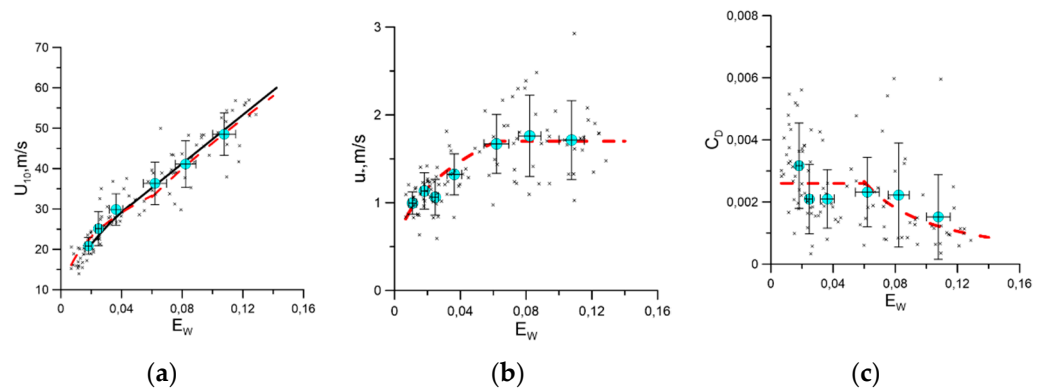$$U_{10} = \begin{cases} 85 E_w^{1/3}, E_w \leq 0.06, \\ 215 E_w^{2/3}, E_w > 0.06 \end{cases} , \tag{13}$$

(a)   (b)   (c)

Figure 6. Comparison of the surface wind speed (**a**), the wind friction velocity (**b**), and drag coefficient of the ocean surface (**c**), retrieved from the data of falling GPS-dropsondes. Small symbols are the results of calculations for individual statistical ensembles composed of velocity profiles measured under approximately the same conditions, large symbols are averaged values, lines of approximation by (13)–(15) are on the right, middle and left panels, respectively. The dotted line on the left panel is the GMF from [19].

It allows a uniform description of the empirical relationships between E_w and two other dynamic characteristics of the atmospheric boundary layer that can be obtained independently on the basis of processing data from the falling GPS dropsondes, u_* (Figure 6b), and C_D (Figure 6c). Similar to Formula (13), the approximations of the dependences $u_*(E_w)$ and $C_D(E_w)$ using two power functions have the form:

$$u_* = \begin{cases} 4.3 E_w^{1/3}, E_w \leq 0.06, \\ 1.7, E_w > 0.06 \end{cases} , \tag{14}$$

$$C_D = \begin{cases} 0.0026, E_w \leq 0.06, \\ 6.25 \cdot 10^{-5} E_w^{-4/3}, E_w > 0.06 \end{cases} , \tag{15}$$

Formulas (13)–(15) are consistent with each other and are in agreement with the data in Figure 6.

Figure 7 illustrates the retrieval of the atmospheric boundary layer dynamic parameters using the expressions (13)–(15), and the ocean surface emissivity is measured using SFMR. The values retrieved are for the surface wind speed U_{10}, the dynamic wind speed u_*, and the drag coefficient C_D along the flight path crossing the eye of hurricane Irma on 2017/09/07. A small difference in the values of the surface wind speed, obtained by formula (13) and the method reported in [6], can be observed in Figure 7. This is the result of the fact that the data set for the analysis used in obtaining expressions (13)–(15) did not include data for the region of low and moderate wind speeds with values of less than 15 m/s, so the obtained expressions are not applicable for the eye of the tropical cyclone, where low wind speeds are observed.
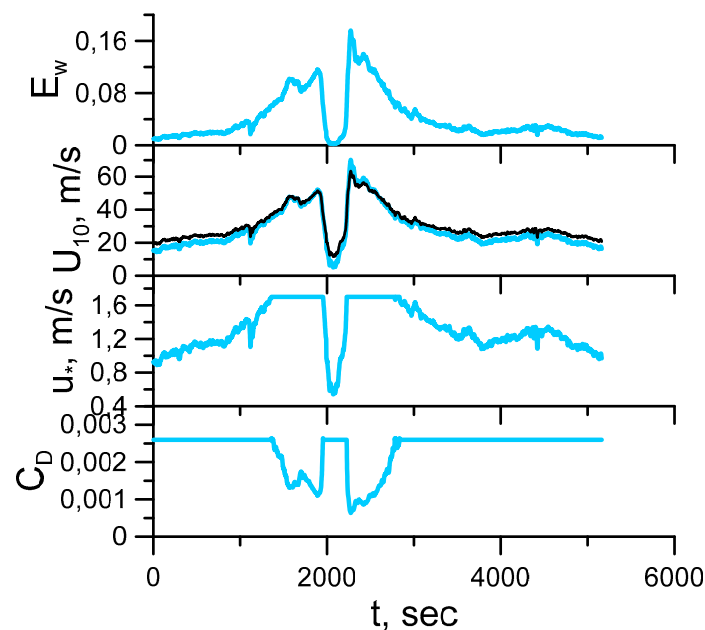

Figure 7. Emissivity of the ocean surface E_w, measured along the track of an aircraft over hurricane Irma 2017/09/07 (1st graph). Blue lines—retrieved values of the surface wind speed (Equation (13), graph 2), the wind friction velocity (Equation (14), graph 3), drag coefficient (Equation (15), graph 4). The black line on the 2nd graph is the surface wind speed retrieved by the algorithm, reported in [19].

Some differences between the surface wind speed obtained by expression (13) and by the algorithm reported in [19] for high wind speeds are also observed. These have probably been introduced by a lack of data and the resulting statistical errors.

It is seen from Equation (14) that the friction wind speed is constant when the emissivity is high (it corresponds to the wall of the tropical cyclone); this is the result of the saturation effect observed in the dependency of $u_*(U_{10})$ at $U_{10} > 35$ m/s (see Figure 5). It should be noted that if additional data are analyzed in the future, a weak dependence $u_*(E_w)$ may be observed. A feature of the drag coefficient is the significant decrease in its values in the area of the wall of the hurricane, where the highest wind speeds are observed. Moreover, in the region of relatively weak winds, it is constant. This is also a consequence of using a limited dataset and will likely be overcome when expanded.

5. The Algorithm for Retrieving Atmospheric Boundary Layer Dynamic Parameters in a Hurricane Based on Collocated Sentinel-1 and SFMR Data

The measurements from the SFMR described in the previous section have been used for the qualitative and quantitative refinement of the obtained dependences of the cross-pol NRCS from Sentinel-1 SAR images on the wind speed and turbulent stress [24]. The

NRCS was determined by averaging in cells of 2×2 km at each point of the aircraft track (Figure 8). The resulting dependences of the NRCS (overall dataset contains 2642 values) on the binned and averaged ocean surface emissivity E_w (binning was made for every 100 values of E_w) are illustrated in Figure 9a.

Figure 8. The track of the aircraft over hurricane Irma superimposed on the Sentinel-1 image 2017/09/07.
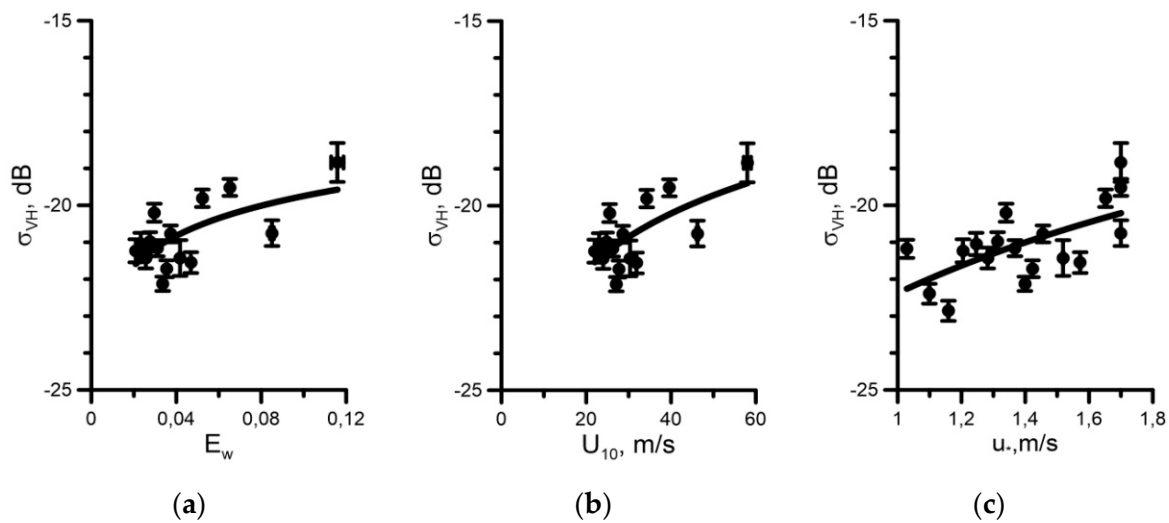

(a)   **(b)**   **(c)**

Figure 9. NRCS dependency on E_w (**a**); U_{10} (**b**); and u_* (**c**) for hurricanes Maria (2017/09/18–2017/09/27, Category 5 (SSHS)) and Irma (2017/09/03–2017/09/10), obtained using collocated satellite data and analysis of measurement results from SFMR and NOAA GPS-dropsondes. Solid lines—logarithmic approximation.

The dependences of the NRCS on the wind speed and on the wind friction speed were obtained using the relations between the SFMR data and the atmospheric boundary layer dynamic parameters (13) (14) from the previous section (see Figure 9b,c).

Similar dependences of the NRCS on the surface wind speed and friction velocity based on a comparison of remote sensing data from the Sentinel-1 satellite with the measurements from GPS-dropsondes were previously obtained by the authors in [24]. The main problem of the approach proposed in [24] was the lack of data acquired by the GPS-dropsondes exactly at the time of the satellite image. Therefore, in order to form a statistical ensemble for averaging, the data from GPS-dropsondes for one day earlier and one day later than

the image were used, with the assumption being made that the hurricane remained quasi-stationary during this period of time. This assumption is only valid for powerful Category 5 hurricanes, while it may not be true for Category 4 or 3 hurricanes in most cases. The main advantage of the proposed approach in comparison with the previously obtained dependences [24] is that the large array of data from the SFMR allows us to obtain more statistics, as the data for processing is acquired exactly on the day of the image, and the hurricane does not change significantly during the measurement period.

6. Discussion

The retrieval of dynamic atmospheric boundary layer parameters, i.e., the surface wind speed, the wind friction velocity, and the aerodynamic drag coefficient, on the basis of collocated measurements from NOAA GPS-dropsondes and SFMR for hurricane conditions has been considered. The analysis was made for 20 Category 4 and 5 tropical cyclones observed during the hurricane seasons 2001–2017 in the Atlantic basin. To obtain the dynamic parameters of the atmospheric boundary layer from the GPS-dropsonde measurements, an algorithm based on the self-similarity of the velocity profile in the boundary layer was used. This algorithm had previously been applied by the authors to determine the wind parameters from the measurements made in the wake part of the boundary layer in a wind wave flume [26].

Based on a comparison of the data obtained from the GPS-dropsondes and measurements with the SFMR, a method has been proposed for retrieval of the parameters of the atmospheric boundary layer from the data on ocean surface emissivity. This method differs from the traditional approach, in which first the wind speed is retrieved from the radiometric data and then the value of the dynamic wind speed is estimated with the "bulk formulas". This method has a significant drawback, since the $C_D(U_{10})$ dependence is non-linear, and in addition, the C_D and U_{10} values were obtained for averaged wind speed profiles under different conditions. The approach proposed in this paper is based on the reconstruction of all the wind parameters based on the E_w measured "here and now".

We should note that the empirical dependences that relate the emissivity of the ocean surface with the dynamic parameters of the atmospheric boundary layer proposed in this paper are preliminary. In order to refine them (in particular, in the region of wind speeds above 35 m/s), an extended data set will be considered in the future.

At the final stage of research, we considered the measurements from the SFMR collocated with SAR images obtained from the Sentinel-1 satellite for hurricane Maria (2017/09/18–2017/09/27, Category 5 (SSHS)) and Irma (2017/09/03–2017/09/10, Category 5 (SSHS)). A relationship was obtained between the emissivity of the ocean surface and the NRCS, and then, based on the proposed method for reconstructing the atmospheric boundary layer data from radiometric measurements, the dependencies of the NRCS on wind speed and turbulent stress (friction velocity) were proposed. These relationships could be used as the basis for further qualitative and quantitative improvement of the methods for the retrieval of atmospheric boundary layer parameters from satellite remote sensing data previously proposed by the authors [24].

Conflicts of Interest: The authors declare no conflict of interest.

References

1. Geernaert, G.L.; Plant, W.J. *Surface Waves and Fuxes*; Kluwer Academic Publishers: Norwell, MA, USA, 1990.
2. Du, Y.; Yang, X.; Yang, J.; Tan, S.; Ma, W.; Li, Z.; Li, X. Effects of Temperature on Sea Surface Radar Backscattering under Neutral and Non-neutral Atmospheric Conditions for Wind Retrieval Applications: A Numerical Study. *IEEE Trans. Geosci. Remote Sens.* **2021**, *59*, 2727–2743. [CrossRef]
3. Garratt, J.R. Review of drag coefcients over oceans and continents. *Mon. Weather. Rev.* **1977**, *105*, 915–929. [CrossRef]
4. Smith, S.D. Coefcients for sea surface wind stress, heat fux, and wind profles as a function of wind speed and temperature. *J. Geophys. Res.* **1988**, *93*, 15467–15472. [CrossRef]
5. Donelan, M.A. Air–sea interaction. In *The Sea*; Ocean Engineering, Science; LeMehaute, B., Hanes, D.M., Eds.; Wiley-Interscience Publisher: Hoboken, NJ, USA, 1990; Volume 9, pp. 239–292.
6. Jones, I.S.F.; Toba, Y. *Wind Stress over the Ocean*; Cambridge University Press: Cambridge, UK, 2001.
7. Wu, J. Wind-stress coefcients over sea surface near neutral conditions—A revisit. *J. Phys. Oceanogr.* **1980**, *10*, 727–740. [CrossRef]
8. Smith, S.D. Wind stress and heat fux over the ocean in gale force winds. *J. Phys. Oceanogr.* **1980**, *10*, 709–726. [CrossRef]
9. Large, W.G.; Pond, S. Open ocean momentum fux measurements in moderate to strong winds. *J. Phys. Oceanogr.* **1981**, *11*, 324–336. [CrossRef]
10. Donelan, M.A.; Drennan, W.M.; Katsaros, K.B. The air–sea momentum fux in conditions of wind sea and swell. *J. Phys. Oceanogr.* **1997**, *27*, 2087–2099. [CrossRef]
11. Edson, J.B.; Venkata, V.; Weller, R.A.; Bigorre, S.P.; Plueddemann, A.J.; Fairall, C.W.; Miller, S.D.; Mahrt, L.; Vickers, D.; Hersbach, H. On the exchange of momentum over the open ocean. *J. Phys. Oceanogr.* **2013**, *43*, 1589–1610. [CrossRef]
12. Powell, M.D.; Vickery, P.J.; Reinhold, T.A. Reduced drag coefficient for high wind speeds in tropical cyclones. *Nature* **2003**, *422*, 279–283. [CrossRef]
13. Donelan, M.A.; Haus, B.K.; Reul, N.; Plant, W.J.; Stiassnie, M.; Graber, H.C.; Brown, O.B.; Saltzman, E.S. On the limiting aerodynamic roughness of the ocean in very strong winds. *Geophys. Res. Lett.* **2004**, *31*, L18306. [CrossRef]
14. Takagaki, N.; Komori, S.; Suzuki, N.; Iwano, K.; Kuramoto, T.; Shimada, S.; Kurose, R.; Takahashi, K. Strong correlation between the drag coefcient and the shape of the wind sea spectrum over a broad range of wind speeds. *Geophys. Res. Lett.* **2012**, *39*, L23604. [CrossRef]
15. Jarosz, E.; Mitchell, D.A.; Wang, D.W.; Teague, W.J. Bottom-Up Determination of Air-Sea Momentum Exchange Under a Major Tropical Cyclone. *Science* **2007**, *315*, 1707–1709. [CrossRef]
16. Holthuijsen, L.H.; Powell, M.D.; Pietrzak, J.D. Wind and waves in extreme hurricanes. *J. Geophys. Res.* **2012**, *117*, C09003. [CrossRef]
17. Bell, M.M.; Montgomery, M.T.; Emanuel, K.A. Air-Sea En-thalpy and Momentum Exchange at Major Hurricane Wind Speeds Observed during CBLAST. *J. Atmos. Sci.* **2012**, *69*, 3197–3222. [CrossRef]
18. Richter, D.H.; Bohac, R.; Stern, D.P. An assessment of the flux profile method for determining Air–Sea momentum and enthalpy fluxes from dropsonde data in tropical cyclones. *J. Atmos. Sci.* **2016**, *73*, 2665–2682. [CrossRef]
19. Uhlhorn, E.W.; Black, P.G. Verification of remotely sensed sea surface winds in hurricanes. *J. Atmos. Ocean. Technol.* **2003**, *20*, 99–116. [CrossRef]
20. Hersbach, H.; Stoffelen, A.; de Haan, S. An improved C-band scatterometer ocean geophysical model function: CMOD5. *J. Geophys. Res.* **2007**, *112*, C03006. [CrossRef]
21. Vachon, P.W.; Wolfe, J. C-band cross-polarization wind speed retrieval. *IEEE Geosci. Remote Sens. Lett.* **2011**, *8*, 456–459. [CrossRef]
22. van Zadelhoff, G.-J.; Stoffelen, A.; Vachon, P.W.; Wolfe, J.; Horstmann, J.; Rivas, M.B. Scatterometer Hurricane Wind Speed Retrievals Using Cross Polarization. *Atm. Measur. Tech. Discuss.* **2013**, *7*, 7945–7984.
23. Zhang, B.; Perrie, W. Cross-polarized synthetic aperture radar: A new potential measurement technique for hurricanes. *Bull. Am. Meteorol. Soc.* **2012**, *93*, 531–541. [CrossRef]
24. Ermakova, O.; Sergeev, D.; Rusakov, N.; Poplavsky, E.; Balandina, G.; Troitskaya, Y. Toward the GMF for Wind Speed and Surface Stress Retrieval in Hurricanes Based on the Collocated GPS-Dropsonde and Remote Sensing Data. *IEEE J. Sel. Top. Appl. Earth Obs. Remote Sens.* **2020**, *13*, 4803–4808. [CrossRef]
25. Hintze, J.O. *Turbulence: An Introduction to Its Mechanism and Theory*; McGraw-Hill: New York, NY, USA, 1959; p. 586.
26. Kandaurov, A.A.; Troitskaya, Y.I.; Sergeev, D.A.; Vdovin, M.I.; Baidakov, G.A. Average velocity field in the air flow over the water surface in laboratory study of the hurricane conditions. *Izv. Atmos. Ocean. Phys.* **2014**, *50*, 399–410. [CrossRef]
27. Franklin, J.L.; Black, M.L.; Valde, K. GPS dropwindsonde wind profiles in hurricanes and their operational implications. *Weather Forecast.* **2003**, *18*, 32–44. [CrossRef]
28. Troitskaya, Y.; Sergeev, D.; Kandaurov, A.; Baidakov, G.; Vdovin, M.; Kazakov, V. Laboratory and theoretical modeling of air-sea momentum transfer under severe wind conditions. *J. Geophys. Res.* **2012**, *117*, C00J21. [CrossRef]
29. Zavadsky, A.; Shemer, L. Characterization of turbulent air flow over evolving water-waves in a wind-wave tank. *J. Geophys. Res.* **2012**, *117*, C00J19. [CrossRef]
30. Kudryavtsev, V.N.; Makin, V.K. Aerodynamic roughness of the sea surface at high winds. *Bound. Layer Meteorol.* **2007**, *125*, 289–303. [CrossRef]

31. Foreman, R.J.; Emeis, S. Revisiting the Definition of the Drag Coefficient in the Marine Atmospheric Boundary Layer. *J. Phys. Oceanogr.* **2010**, *40*, 2325–2332. [CrossRef]

32. Troitskaya, Y.; Druzhinin, O.; Kozlov, D.; Zilitinkevich, S. "Bag-breakup" spume droplet generation mechanism at hurricane wind. Part II. Contribution to momentum and enthalpy transfer. *J. Phys. Oceanogr.* **2018**, *48*, 2189–2207. [CrossRef]

33. Golbraikh, E.; Shtemler, Y.M. Foam input into the drag coefficient in hurricane conditions. *Dynam. Atmos. Ocean* **2016**, *73*, 1–9. [CrossRef]

34. Troitskaya, Y.; Sergeev, D.; Kandaurov, A.; Vdovin, M.; Zilitinkevich, S. The Effect of Foam on Waves and the Aerodynamic Roughness of the Water Surface at High Winds. *J. Phys. Oceanogr.* **2019**, *49*, 959–981. [CrossRef]

35. Bender, M.A.; Ginis, I. Real-Case Simulations of Hurricane–Ocean Interaction Using a High-Resolution Coupled Model: Effects on Hurricane Intensity. *Mon. Weather Rev.* **2000**, *128*, 917–946. [CrossRef]